Lithium-Ion Batteries

Deutsche Ausgabe: DOI: 10.1002/ange.201511196
Internationale Ausgabe: DOI: 10.1002/anie.201511196

A General and Mild Approach to Controllable Preparation of Manganese-Based Micro- and Nanostructured Bars for High Performance Lithium-Ion Batteries

Guo Ma[+], Sheng Li[+], Weixin Zhang, Zeheng Yang, Shulin Liu, Xiaoming Fan, Fei Chen, Yuan Tian, Weibo Zhang, Shihe Yang,* and Mei Li*

Abstract: *One-dimensional (1D) micro- and nanostructured electrode materials with controllable phase and composition are appealing materials for use in lithium-ion batteries with high energy and power densities, but they are challenging to prepare. Herein, a novel ethanol–water mediated co-precipitation method by a chimie douce route (synthesis conducted under mild conditions) has been exploited to selectively prepare an extensive series of manganese-based electrode materials, manifesting the considerable generalizability and efficacy of the method. Moreover, by simply tuning the mixed solvent and reagents, transition metal oxide bars with differing aspect ratios and compositions were prepared with an unprecedented uniformity. Application prospects are demonstrated by Li-rich* $0.5\,Li_2MnO_3{\cdot}0.5\,LiNi_{1/3}Co_{1/3}Mn_{1/3}O_2$ *bars, which demonstrate excellent reversible capacity and rate capability thanks to the steerable nature of the synthesis and material quality. This work opens a new route to 1D micro- and nanostructured materials by customizing the precipitating solvent to orchestrate the crystallization process.*

To meet the requirements of large-scale applications in electric vehicles, hybrid vehicles and stationary energy storage, research efforts have been directed towards economic, sustainable and environmentally friendly methods for production of electrode materials for rechargeable lithium-ion batteries (LIBs), which have high energy and power densities.[1]

Manganese-based electrode materials, such as layered $LiNi_xCo_{1-x-y}Mn_yO_2$,[2] spinel $LiNi_{0.5}Mn_{1.5}O_4$,[3] and layered Li-rich $x\,Li_2MnO_3{\cdot}(1-x)LiNi_{1/3}Mn_{1/3}Co_{1/3}O_2$ $(0 \le x \le 1)$[4] have undergone a flurry of research because of their high energy and power density advantages, as well as their low cost and high cycling performance in LIBs.

Electrodes comprising 1D micro- and nanostructured materials exhibit outstanding electrochemical performances owing to the shortening of electron and lithium diffusion paths, an appropriate contact area between active materials and electrolyte, and their ability to accommodate strain (which is related to compliancy towards structural transformation upon repeated Li^+ insertions and extractions).[5,6] Much effort has been expended on the synthesis of 1D micro- and nanostructured materials. For example, a micro-emulsion method has been reported for preparation of MnC_2O_4 nanorods as precursors for fabrication of $LiNi_{0.5}Mn_{1.5}O_4$ porous nanorods with diameters of 100–400 nm and lengths of $>10\,\mu m$. The materials produced displayed discharge capacities of 140 and 109 $mAh\,g^{-1}$ at 1 C and 20 C rates, respectively.[5b] $Co_{0.4}Mn_{0.6}O_2$ nanowires were also reported as precursors for hydrothermally produced $Li_{0.88}[Li_{0.18}Co_{0.33}Mn_{0.49}]O_2$ nanowires with diameters of 100 nm and lengths of $>3\,\mu m$, which had discharge capacities of 245 and 230 $mAh\,g^{-1}$ at rates of 0.2 C and 5 C, respectively.[6b]

In respect to thermal stability, Dahn and co-workers[7] recently showed that larger particles with a higher tap density would be less reactive in a highly oxidized state. On the other hand, an electrode comprising consistently and appropriately sized particles could ensure uniform reversible intercalation over repeated cycles.[8] Therefore, tailoring of lithium-ion battery electrode materials by control of particle size and morphology has received growing attention in recent years. To date, it has remained a challenge to develop a general strategy that allows large-scale preparation of a wide array of 1D micro- and nanostructured manganese-based electrode materials with a controllable phase, composition and shape, as well as a narrow size distribution.

Herein, we propose a facile, general, and mild approach for fabricating 1D micro- and nanostructured manganese-based electrode materials with high energy and power densities, by judiciously formulating a precipitating solvent. Specifically, uniform metal oxalate hydrate ($MC_2O_4{\cdot}x\,H_2O$; M = Mn, Ni, Co, Li, Zn) microbars were prepared by

[*] G. Ma,[+] S. Li,[+] Prof. Dr. W. X. Zhang, Prof. Dr. Z. H. Yang, S. L. Liu, Dr. X. M. Fan, F. Chen, Y. Tian, W. B. Zhang
School of Chemistry and Chemical Engineering, Hefei University of Technology, Anhui Key Laboratory of Controllable Chemical Reaction & Material Chemical Engineering
Hefei, Anhui 230009 (P.R. China)
E-mail: wxzhang@hfut.edu.cn
Prof. Dr. S. H. Yang
Department of Chemistry, William Mong Institute of Nano Science and Technology, The Hong Kong University of Science and Technology
Clear Water Bay, Kowloon, Hong Kong (P.R. China)
E-mail: chsyang@ust.hk
Dr. M. Li
School of Chemistry, Centre for Organized Matter Chemistry, University of Bristol
Bristol BS8 1TS (UK)
[+] These authors contributed equally to this work and should be considered as co-first authors.

Supporting information for this article is available on the WWW under http://dx.doi.org/10.1002/anie.201511196.

precipitation in an optimized ethanol–water co-solvent at room temperature. The subsequent post-annealing treatment topotactically converted the precursor to the target electrode material with an overall conservation of morphology. We were able to tune aspect ratios of the $MC_2O_4{\cdot}x\,H_2O$ microbars by controlling the volume ratio of ethanol–water in the co-precipitation reaction. This co-solvent tuning strategy is based on adjusting kinetics of crystallite nucleation and growth related to the variation of dielectric constant, among other things, with the ethanol–water ratio of the precipitating solvent. We show the generality of our method and its usefulness for developing high performance lithium-ion batteries.

We chose layered Li-rich $0.5\,Li_2MnO_3{\cdot}0.5\,LiNi_{1/3}Co_{1/3}Mn_{1/3}O_2$ as an example to demonstrate the effectiveness of this method at producing 1D micro- and nanostructures as electrodes for LIBs. Scheme 1 illustrates our strategy for generating $0.5\,Li_2MnO_3{\cdot}0.5\,LiNi_{1/3}Co_{1/3}Mn_{1/3}O_2$ porous micro- and nanostructured bars, involving a co-precipitation step mediated by mixed solvent, and a subsequent post-heat treatment. Uniform metal oxalate microbars $MC_2O_4{\cdot}2\,H_2O$ were only obtained with a certain ratio of ethanol–water in the mixed solvent. Note that the co-precipitation reaction was carried out at room temperature without use of any surfactant. The precursor was then transformed into manganese-based electrode materials by post-heat treatment, with good retention of overall morphology.

Use of an ethanol–water mixed solvent for synthesis of precursors capitalizes on a composition-dependent change in dielectric constant and solvation power, which would have an impact on supersaturation and kinetics, and thus on the activation free energy for nucleation. In water, reduction of the dielectric constant and alteration of solute–solvent interactions can be accomplished by adding ethanol, thereby adjusting the relative order of reaction kinetics for Ni, Co, and Mn, and their supersaturation,[9] which may lower the nucleation barrier and thus facilitate co-precipitation.[10] Indeed, solvent effects on all the metallic ions in solution (Mn^{2+}, Ni^{2+}, Co^{2+}, and Li^+) can be regulated by tuning the volume ratio of ethanol to water in the mixed solvent.

FESEM and TEM images in Figure 1 show that the calcined $0.5\,Li_2MnO_3{\cdot}0.5\,LiNi_{1/3}Co_{1/3}Mn_{1/3}O_2$ product (Supporting Information, Figure S1, α-$NaFeO_2$ type layered structure) is composed of uniform micro- and nanostructured bars with lengths of 6.4 ± 0.4 μm and widths of 1.2 ± 0.2 μm, which retain the rectangular bar-like architectures of the $MC_2O_4{\cdot}x\,H_2O$ precursor obtained during nucleation in an ethanol–water mixture (volume ratio of $R=5{:}1$, Figure 1a; Supporting Information, Figure S2, Figure S13e,f).[11] The product specific surface area ($6.76\ m^2g^{-1}$; Supporting Information, Figure S3) is bigger than that of the precursor ($2.79\ m^2g^{-1}$) owing to formation of pores and void spaces (Figure 1b–d) during the calcination process. The HRTEM image (Figure 1e) combined with the corresponding selected-area fast Fourier transform (FFT) pattern (Figure 1f) further confirms that the as-prepared product is composed of a layered $LiNi_{1/3}Co_{1/3}Mn_{1/3}O_2$ (space group $R\bar{3}m$) and Li_2MnO_3 component (space group $C/2m$), and the marked lattice fringe spacing of 0.47 nm corresponds to (003) planes of $0.5\,Li_2MnO_3{\cdot}0.5\,LiNi_{1/3}Co_{1/3}Mn_{1/3}O_2$.[4a,b] Moreover, element mapping (Figure 1g) shows that Mn, Co, and Ni elements distribute uniformly across the micro- and nanostructured bars. The atomic ratios of Mn, Co, and Ni detected from the EDS spectrum are close to 4:1:1 (Figure 1h), in good agreement with the theoretical ratio of elements in $0.5\,Li_2MnO_3{\cdot}0.5\,LiNi_{1/3}Mn_{1/3}Co_{1/3}O_2$.

Several control experiments were conducted to determine the effect of ethanol (low dielectric constant) on the precipitating solvent, and on the formation of $MC_2O_4{\cdot}x\,H_2O$ precursors. First, it was found that the precipitating solvent became turbid faster using a mixed ethanol–water solvent than with pure water, indicating a higher precipitation rate in a mixed solvent (Supporting Information, Figure S4). Second, when three metal ion solutions (exclusively containing Mn^{2+}, Ni^{2+}, or Co^{2+}, in 5:1 ethanol–water) were added separately to three identical oxalic acid ethanol–water (5:1 volume ratio) solutions, the turbidity of the Mn^{2+} solution increased rapidly. By comparison, Ni^{2+} and Co^{2+} solutions became turbid slowly after an initial small rise in turbidity, indicating that a large quantity of MnC_2O_4 was first precipitated from the nascent reaction mixture in the presence of all metal ions (Supporting Information, Figure S5e). In contrast, turbidity change versus time in aqueous solution indicates that the rate of CoC_2O_4 generation is much higher than that for MnC_2O_4 and NiC_2O_4 (Supporting Information, Figure S5f). Significantly, addition of ethanol has a strong solvent effect on the Mn^{2+}, Ni^{2+}, and Co^{2+} ions; it changes their apparent concentrations and thus alters supersaturation and modifies the kinetics of crystallite nucleation. Comparatively, the rate of NiC_2O_4 generation was

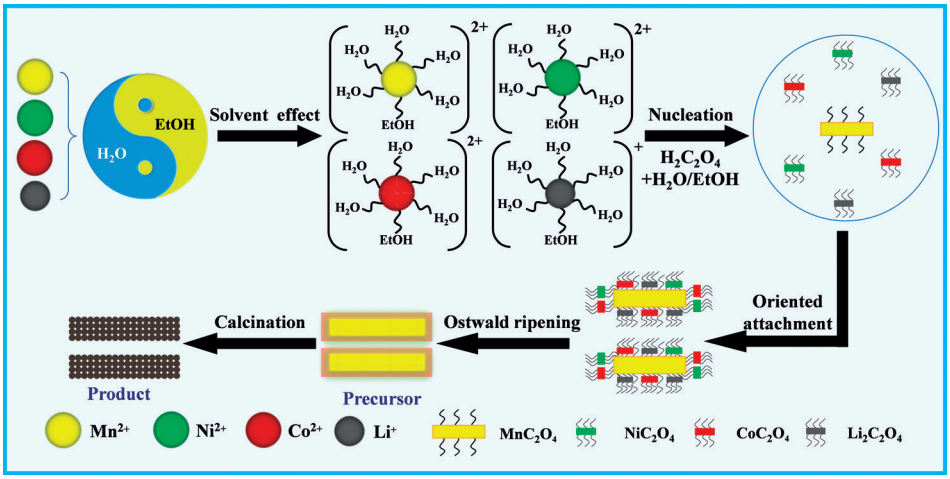

Scheme 1. Illustration of ethanol mediated co-precipitation coupled with subsequent calcination for the formation of $0.5\,Li_2MnO_3{\cdot}0.5\,LiNi_{1/3}Co_{1/3}Mn_{1/3}O_2$ 1D porous micro- and nanostructured bars.

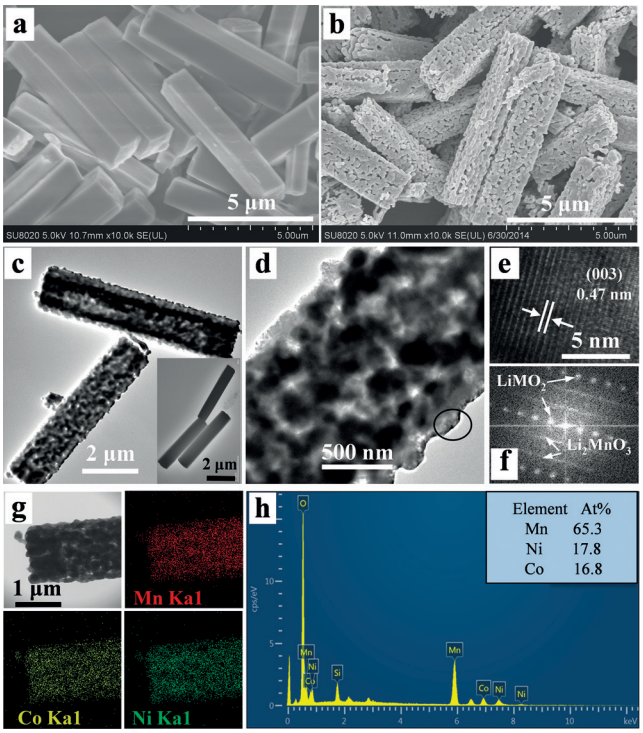

Figure 1. FESEM images of a) $MC_2O_4{\cdot}xH_2O$ (M = Mn, Ni, Co, Li) precursor and b) $0.5\,Li_2MnO_3{\cdot}0.5\,LiNi_{1/3}Co_{1/3}Mn_{1/3}O_2$ product; c, d) TEM and HRTEM images of the product (inset of c: TEM image of precursor); e) HRTEM image of the circled region in (d); f) FFT of the HRTEM image in (e); g) Element mapping (Mn, Co, and Ni); h) EDS spectrum of the tip of a $0.5\,Li_2MnO_3{\cdot}0.5\,LiNi_{1/3}Mn_{1/3}Co_{1/3}O_2$ microbar ($R = 5{:}1$).

extremely low in both aqueous and mixed solutions, even after addition of ethanol to accelerate the reaction kinetics.

Note that, although CoC_2O_4 has a greater generation rate than MnC_2O_4 in aqueous solution, the first precipitated CoC_2O_4 seeds could not template the MC_2O_4 precursor as the newly formed MnC_2O_4 nanobar seeds[12] do in the mixed solution (Supporting Information, Figure S6,7). MnC_2O_4 nanobar seeds serve as templates for recruiting and assimilating other metal oxalates by oriented attachment and Ostwald ripening, yielding $MC_2O_4{\cdot}2H_2O$ microbars. EDS spectra and elemental mapping of $MC_2O_4{\cdot}xH_2O$ precursor collected after different reaction times indicates that MnC_2O_4 nanobars formed first in the ethanol–water system, whereas CoC_2O_4 and NiC_2O_4 existed as nanoflakes (Supporting Information, Figures S8–S10). Over time, manganese accumulates in high concentrations in the main body of MnC_2O_4 nanobars while nickel and cobalt attach to the exterior. Line-scanning EDS and mapping of Ni, Co, and Mn elements of $MC_2O_4{\cdot}xH_2O$ microbar precursor along the transverse and axial directions (Supporting Information, Figure S11), confirm that Co and Ni elements are located on the exterior of the microbar, whereas Mn presides in the center. Clearly, the microbar product is characterized by segregation of transition metal ions, reflecting the unique growth mechanisms in operation.

To verify the templating role played by $MnC_2O_4{\cdot}2H_2O$ microbars, we changed the addition order of reagents by a stepwise co-precipitation[5c] using the same ethanol–water volume ratio of $R = 5{:}1$. The results demonstrate that the obtained $MC_2O_4{\cdot}2H_2O$ precipitate has a similar rectangular bar morphology to that of the precipitated $MnC_2O_4{\cdot}2H_2O$ described above (Supporting Information, Figure S12).

On the other hand, the impacts of the ethanol–water volume ratios (R) on the morphologies of $MC_2O_4{\cdot}xH_2O$ precursors (S1, S2, S3, and S4) have been investigated (Supporting Information, Figure S13, Table S1). When ethanol was added to aqueous solution in ratios of $R = 0{:}1$, 1:3, 5:1, and 24:1, the dielectric constants of the mixed solvents were 78, 60, 32, and 24,[10] respectively. The decreasing dielectric constant reduces solubility and increases supersaturation of the solutes, which could affect the thermodynamics and nucleation kinetics of the crystallite formation in the reaction system, and have a significant effect on crystallite growth because of changes to solute–solvent interactions. As a result, not only has the precipitation order been changed for the metal oxalates, but the reaction (precipitation) speed was also accelerated with the addition of ethanol. Ethanol molecules behaving like mini-surfactants might be selectively adsorbed on specific crystallite faces, allowing metal oxalate crystallites to grow in one dimension. Higher ethanol–water volume ratios provide increased concentrations of ethanol molecules, thereby directing the growth of crystallite into longer microbars.

Four $0.5\,Li_2MnO_3{\cdot}0.5\,LiNi_{1/3}Co_{1/3}Mn_{1/3}O_2$ 1D micro- and nanostructured bars (LNCM-1, LNCM-2, LNCM-3, and LNCM-4; Supporting Information, Figures S14 and S15) were obtained by post-heat treatment of the four corresponding $MC_2O_4{\cdot}xH_2O$ precursor precipitates (S1, S2, S3, and S4). Material morphologies were conserved for all products (Figure 1a; Supporting Information, Figure S13).

Ethanol mediated co-precipitation coupled with subsequent post-heat treatment can be easily extended to other manganese-based electrode materials. By tuning the parameters of reagents and mixed ethanol–water solvent, a series of precursors and manganese-based electrode materials with uniform 1D porous micro- and nanostructured bar morphologies were prepared. These include Li-rich $0.5\,Li_2MnO_3{\cdot}0.5\,LiNi_{0.5}Mn_{0.5}O_2$, layered $LiNi_{1/3}Co_{1/3}Mn_{1/3}O_2$, spinel $LiNi_{0.5}Mn_{1.5}O_4$ and $LiMn_2O_4$ cathode materials, and spinel $NiMn_2O_4$ and $ZnMn_2O_4$ anode materials (Figure 2; Supporting Information, Figures S16–18, Table S2).

To demonstrate the application value of the 1D micro- and nanostructured manganese-based materials, the four samples LNCM-1, LNCM-2, LNCM-3, and LNCM-4 were investigated as cathode materials for LIBs. The initial discharge capacity of LNCM-3 reached 297.1 $mAh\,g^{-1}$ with an initial coulombic efficiency of 86.4% at a rate of 0.1 C (Figure 3a), which is markedly enhanced in comparison with the other three samples (Supporting Information, Figure S19) and those previously reported (ca. 80%).[2b,13] LNCM-3 delivers discharge capacities from 269.8–151.0 $mAh\,g^{-1}$, corresponding to a current density range of 0.2–10 C. The potential plateaus and reproducibility of the charge–discharge profiles of LNCM-3 are in good agreement with its differential capacity dQ/dV plots (Figure 3b).

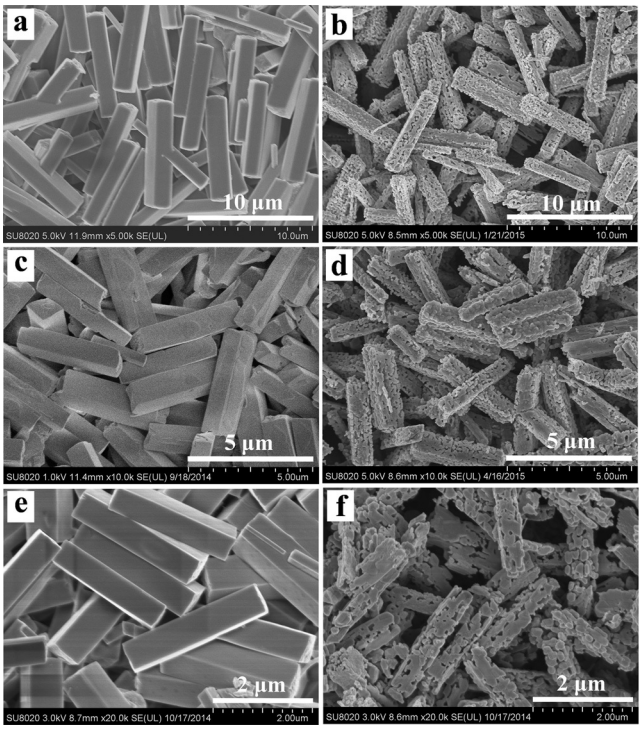

Figure 2. FESEM images of microbars: a) precursor and b) product of layered $0.5\,Li_2MnO_3{\cdot}0.5\,LiNi_{0.5}Mn_{0.5}O_2$; c) precursor and d) product of layered $LiNi_{1/3}Co_{1/3}Mn_{1/3}O_2$; e) precursor and f) product of spinel $LiNi_{0.5}Mn_{1.5}O_4$.

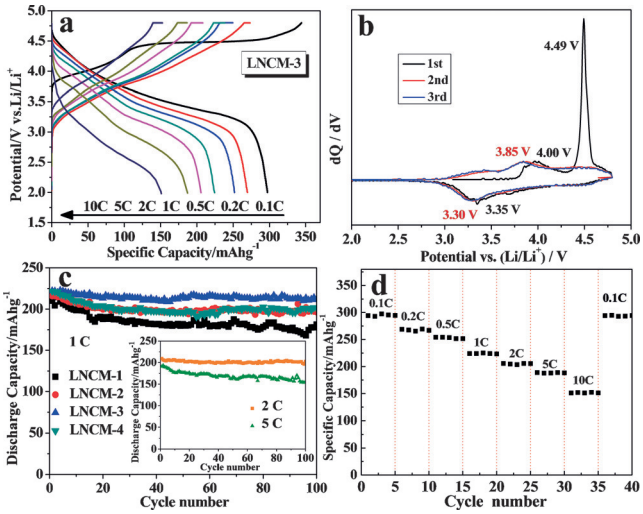

Figure 3. $0.5\,Li_2MnO_3{\cdot}0.5\,LiNi_{1/3}Co_{1/3}Mn_{1/3}O_2$ electrochemical performance (LNCM-3, $R = 5{:}1$) as an LIB cathode material: a) Charge–discharge profiles at various rates in the voltage range of 2.0–4.8 V; b) differential capacity dQ/dV (Q: capacity; V: voltage of the cells) plots at the rate of 0.1 C; c) cycling performances in comparison with the other three samples at a rate of 1 C (inset: cycling performances of LNCM-3 at 2 C and 5 C); d) rate capability at different rates ($1\,C = 250\,mAh\,g^{-1}$).

The cycling performance of cathode materials at high rate is also of significance for practical applications. Figure 3c shows that the discharge capacity of LNCM-3 ($R = 5{:}1$) exhibits a slight decline from 221.9–211.4 $mAh\,g^{-1}$ and higher capacity retention of 95% after 100 cycles at a rate of 1 C (capacity retention for LNCM-1, LNCM-2, and LNCM-4 was 84%, 91%, and 90%, respectively). Moreover, after 100 cycles LNCM-3 can maintain a discharge capacity of 202.8 and 154.2 $mAh\,g^{-1}$ with a capacity retention of 97% and 81% at a rate of 2 C and 5 C, respectively (inset of Figure 3c). Figure 3d further confirms that the LNCM-3 sample exhibits good rate capability; when the rate is decreased from 10 C to 0.1 C, its reversible capacity can recover back to 296 $mAh\,g^{-1}$.

The aforementioned results combined with electrochemical impedance spectroscopy (EIS) tests indicate that, among the four samples, LNCM-3 microbars exhibit the highest reversible capacity and rate capability as well as the best cycling stability (Supporting Information, Figure S20, Table S3). The homogeneous structural units and suitable surface area of LNCM-3 (Supporting Information, Figure S21) may result in regular networks that can maintain a uniform intercalation reversibility in each bar through repeated cycles. Enhanced cycling stability is further supported by preservation of integrity and stability of the electrode (Supporting Information, Figure S22). The unique micro- and nanostructure bars contribute greatly to enhanced performances.[14] Their 1D architecture is advantageous for shortening the electron and lithium diffusion lengths, providing an appropriate contact area between active materials and electrolyte, facilitating efficient diffusion of electrolyte into the inner regions of the electrode, and accommodating the volume changes associated with repeated Li^+ insertion and extraction.

Importantly, the Li-rich $0.5\,Li_2MnO_3{\cdot}0.5\,LiNi_{0.5}Mn_{0.5}O_2$, layered $LiNi_{1/3}Co_{1/3}Mn_{1/3}O_2$, spinel $LiNi_{0.5}Mn_{1.5}O_4$ 1D micro- and nanostructured cathode and $ZnMn_2O_4$ anode materials obtained exhibit excellent electrochemical performances with a high reversible capacity, high rate capability, and improved cycling stability at high current density (Supporting Information, Figure S23–26). These results accentuate the high quality of the products achieved by the present synthesis method. Material quality is an essential consideration when constructing high performance LIBs.

Promisingly, it is very flexible to scale-up the ethanol mediated co-precipitation at a weight ratio of 1:30 (a 30 times enlargement in production capacity) to manufacture the $LiNi_{1/3}Co_{1/3}Mn_{1/3}O_2$ cathode material, without sacrificing their excellent electrochemical performances. The detailed results from the scale-up testing are shown in the Supporting Information, Figure S27.

In conclusion, we have developed a chimie douce approach involving mixed solvent co-precipitation to selectively prepare an extensive series of 1D micro- and nanostructured manganese-based electrode materials. These include cathode and anode materials for LIBs with high energy and power densities, attesting to the generality and effectiveness of the method. Based on kinetic elaboration of crystallite nucleation and growth through mixed solvent mediation, the new route is easily controllable, repeatable, and generally applicable to fabrication of a large series of manganese-based electrode materials with tunable 1D micro-

and nanostructures. Some of these promise enhanced performance once implemented in lithium-ion batteries. In a significant departure from conventional techniques, the present method is conducted in mixed ethanol–water solutions at room temperature, without a need for long-chain surfactants or hydrothermal conditions. Moreover, the method can be employed to produce different aspect ratios of microbars with mixed transition metal oxides by tuning the ethanol–water volume ratio in the solvent. It is anticipated that the mixed solvent mediated co-precipitation strategy will promote heuristic and systematic design of numerous mixed transition metal oxides with controllable phase and composition with desirable micro- and nanostructures for LIB applications.

Acknowledgements

We are grateful for the financial support of the National Natural Science Foundation of China (NSFC Grants 21176054, 21271058 and 91534102).

Keywords: chimie douce approach · electrode materials · lithium-ion batteries · manganese-based micro- and nanostructured bars

How to cite: *Angew. Chem. Int. Ed.* **2016**, *55*, 3667–3671
Angew. Chem. **2016**, *128*, 3731–3735

[1] a) A. S. Aricò, P. Bruce, B. Scrosati, J. M. Tarascon, W. Van Schalkwijk, *Nat. Mater.* **2005**, *4*, 366; b) C. Li, X. P. Han, F. Y. Cheng, Y. X. Hu, C. C. Chen, J. Chen, *Nat. Commun.* **2015**, *6*, 7345, DOI: 10.1038/ncomms8345.

[2] a) T. Ohzuku, Y. Makimura, *Chem. Lett.* **2001**, *30*, 642; b) J. Choi, A. Manthiram, *J. Electrochem. Soc.* **2005**, *152*, A1714; c) W. Liu, P. Oh, X. E. Liu, M. J. Lee, W. Cho, S. Chae, Y. Kim, J. Cho, *Angew. Chem. Int. Ed.* **2015**, *54*, 4440; *Angew. Chem.* **2015**, *127*, 4518.

[3] a) Q. M. Zhong, A. Bonakdarpour, M. J. Zhang, Y. Gao, J. R. Dahn, *J. Electrochem. Soc.* **1997**, *144*, 205; b) W. X. Zhang, G. Ma, H. Y. Gu, Z. H. Yang, H. Cheng, *J. Power Sources* **2015**, *273*, 561.

[4] a) H. J. Yu, H. S. Zhou, *J. Phys. Chem. Lett.* **2013**, *4*, 1268; b) M. M. Thackeray, S. H. Kang, C. S. Johnson, J. T. Vaughey, R. Benedek, S. A. Hackney, *J. Mater. Chem.* **2007**, *17*, 3112; c) N. Yabuuchi, K. Yoshii, S. T. Myung, I. Nakai, S. Komaba, *J. Am. Chem. Soc.* **2011**, *133*, 4404–4419.

[5] a) L. Zhou, D. Y. Zhao, X. W. (David) Lou, *Angew. Chem. Int. Ed.* **2012**, *51*, 239–241; *Angew. Chem.* **2012**, *124*, 243–245; b) X. L. Zhang, F. Y. Cheng, J. G. Yang, J. Chen, *Nano Lett.* **2013**, *13*, 2822; c) Z. H. Yang, J. B. Lu, D. C. Bian, W. X. Zhang, X. N. Yang, J. F. Xia, H. Chen, H. Y. Gu, G. Ma, *J. Power Sources* **2014**, *272*, 144.

[6] a) H. B. Wu, H. Pang, X. W. (David) Lou, *Energy Environ. Sci.* **2013**, *6*, 3619; b) Y. J. Lee, M. G. Kim, J. Cho, *Nano Lett.* **2008**, *8*, 957; c) Y. M. Zhang, W. X. Zhang, Z. H. Yang, H. Y. Gu, Q. Zhu, S. H. Yang, M. Li, *Angew. Chem. Int. Ed.* **2015**, *54*, 3932–3936; *Angew. Chem.* **2015**, *127*, 4004–4008.

[7] S. Jouanneau, K. W. Eberman, L. J. Krause, J. R. Dahn, *J. Electrochem. Soc.* **2003**, *150*, A1637.

[8] Y. G. Guo, J. S. Hu, L. J. Wan, *Adv. Mater.* **2008**, *20*, 2878.

[9] G. Akerlof, *J. Am. Chem. Soc.* **1932**, *54*, 4125.

[10] H. I. Chen, H. Y. Chang, *Colloids Surf. A* **2004**, *242*, 61.

[11] a) Y. Gao, M. V. Yakovleva, W. B. Ebner, *Electrochem. Solid-State Lett.* **1998**, *1*, 117; b) T. Ohzuku, A. Ueda, M. Nagayama, Y. Iwakoshi, H. Komori, *Electrochim. Acta* **1993**, *38*, 1159.

[12] F. Manoli, E. Dalas, *J. Cryst. Growth* **2000**, *218*, 359.

[13] a) Y. Wu, A. Vadivel Murugan, A. Manthiram, *J. Electrochem. Soc.* **2008**, *155*, A635; b) H. Xu, S. Deng, G. Chen, *J. Mater. Chem. A* **2014**, *2*, 15015.

[14] a) K. Xu, *Chem. Rev.* **2004**, *104*, 4303; b) D. Aurbach, *J. Power Sources* **2000**, *89*, 206; c) J. Zhang, R. Wang, X. Yang, W. Lu, X. Wu, X. Wang, H. Li, L. Chen, *Nano Lett.* **2012**, *12*, 2153.

Received: December 3, 2015
Published online: February 15, 2016

